DESY Summer School 2007
Report

Multi-Photon Production at High Transverse Momentum in ep collisions at HERA

Summer Student: Alin VELEA
Supervisor: Cristinel DIACONU

Abstract

Multi-photon production can be measured at high transverse momentum of positron- and electron-proton collisions collected by the H1 experiment at HERA. The production of multiple isolated photons in ep collisions is possible via QED radiation at large angles. The aim of this analysis is to investigate the production rates in the elastic and inelastic cases compared to inclusive NC-DIS and with Compton processes. The Monte Carlo simulation is not describing this data so this investigation based on the data can be the basis for further analysis work.

1 Introduction

1.1 ep scattering

The matter structure is investigated at accelerators using high energy particle scattering. An energetic point-like particle can reveal the structure of an composed object. In addition, new interactions or phenomena can enrich the knowledge of the theory behind the elementary particles. The deep-inelastic scattering (DIS) of an electron and a proton is studied at HERA collider. It has been used to greatly extend the knowledge of the proton structure. A sketch of the DIS process (called Feynmann diagram) is displayed in figure 1.

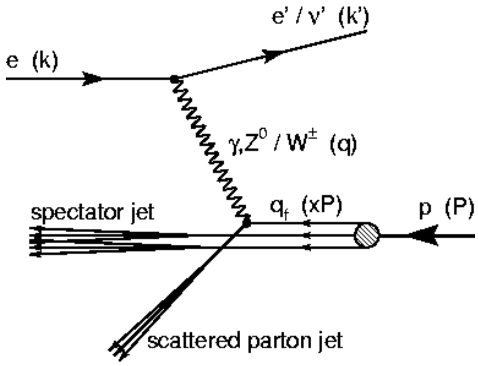

Figure 1: Lepton hadron scattering

The electron e with four momentum k collides with a proton p with four momentum P. At high energy, the structure of the proton is resolved and the electron scatters off a parton wich carries the fractional four momentum x of the proton. The interaction between the electron and the parton is mediated by the exchange of a virtual gauge boson which transfers the four momentum $q = k - k'$. The scattered parton hadronises and produces a jet. The remaining partons proceed along the proton direction and form the remnant or spectator jet. Depending on the charge of the exchanged boson the scattering is a neutral current (NC) or a charged current (CC) interaction.

The present analysis deals with inclusive neutral current deep inelastic ep scattering, a photon γ or Z_0 boson is exchanged.

$$e(k) + p(P) = e'(k') + X \tag{1}$$

The particle's four momentum are given in parentheses. X denotes the hadronic final state wich represent the sum of all final state apart from the scattered electron.
A set of Lorentz invariant kinematic variables are used to describe the process:

$$Q^2 = -q^2 = -(k - k')^2 \tag{2}$$

Q^2 is the virtuality wich is the negative four momentum squared transfered by the virtual photon.

$$x = \frac{Q^2}{2 \times P \times q} \, 0 < x < 1 \tag{3}$$

x is the Bjorken scaling variable. In the Quark Parton Model (QPM) where particle masses and parton transverse momentum are neglected, x is the fraction of the proton momentum carried by the struck parton.

$$y = \frac{P \times q}{P \times k} \; 0 < y < 1 \tag{4}$$

y is the inelasticity variable, which is the fraction of the incident lepton energy carried by the exchanged boson in the proton rest frame.
Neglecting the proton and the lepton masses we obtain next important relation:

$$Q^2 = s \times x \times y \tag{5}$$

where $\sqrt{s}$ is the center of mass energy of the total ep scattering process:

$$s = (p + k)^2 = 4E_e E_p \tag{6}$$

with E_e and E_p, the beam energies of the lepton and the proton. At HERA $\sqrt{s} = 318GeV$ and defines the largest mass of a particle that can be produced on-shell. During the DIS process, photon can be radiated in the initial and final states.

1.2 The radiative scattering

The dominant contributions to radiative elastic ($ep- > e\gamma + p$) and inelastic ($ep- > e\gamma + X$) are described in figure 2. There are three classes of radiative processes [7] coresponding to the kinematic domains defined by the virtual momenta of the propagators:

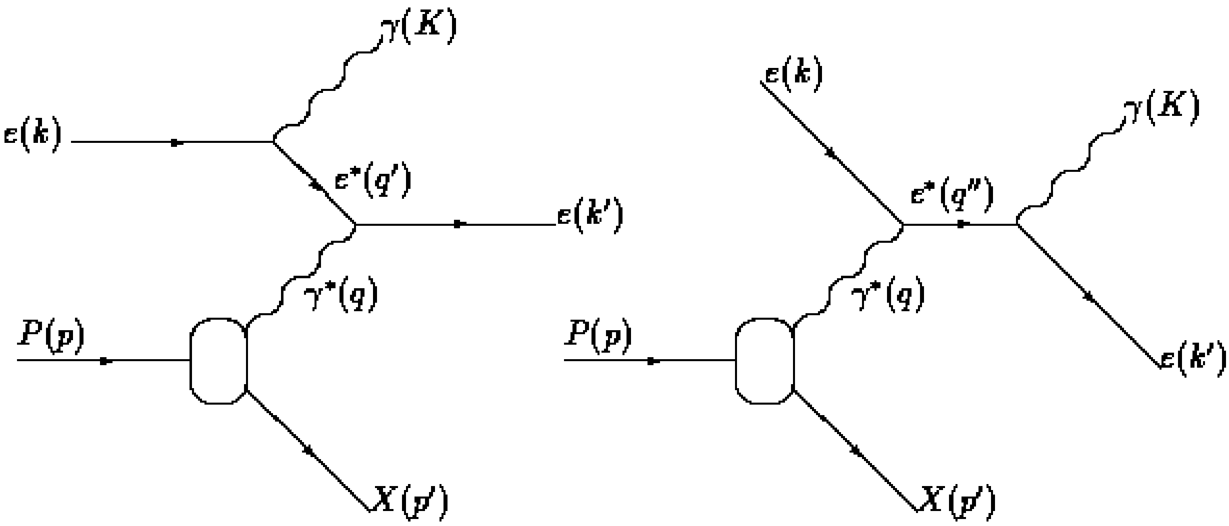

Figure 2: Radiative DIS scattering.

- The bremsstrahlung process

In the bremsstralung process the masses of the virtual photon and of the virtual electron are small $(0 < -q^2, -q'^2, -q''^2 \simeq 0.00015 GeV^2)$. In this kinematic domain the elastic channel is the dominant process. the electron radiates a proton in the electromagnetic field of the proton, which can be regarded as poinlike. Both the outgoing electron and the photon emerge at very small angles with respect to the incident electron direction. The recoil proton continues its motion almost undisturbed. Events of this type are identified either by detecting both the scattered electron and the photon, or by detecting only the photon. In the bremsstrahlung process the energy of the photon (E_γ) and the energy of the scattered electron (E') are constrained:

$$E_e = E'_e + E_\gamma \tag{7}$$

This process is used to measure luminosity at HERA, since the cross section is known to a high precision. The produced photons are detected with dedicated detectors situated close to the beam line.

- The QED Compton process

In the QED Compton process both $-q'^2$ and $-q''^2$ are large $(-q'^2, -q''^2 \simeq 3.5 GeV^2)$ (off-shell electron) and $-q^2$ is small $(-q^2 << -q'^2, -q''^2)$ (quasi-real photon). This process corresponds to the Compton scattering of a quasy-real photon on a incident electron

$$e + \gamma^* - > e + \gamma \tag{8}$$

The dominant contribution to Compton scattering is the due to the elastic channel, but the inelastic contribution is no longer negligible with the respect to the elastic one, but however small. The scattered electron and the photon are observed in the central detector. As $-q^2$ is small, the proton and the $(e - \gamma)$ system have transverse momentum close to zero. The hadronic final state remains undetected in the most of the cases.

- The radiative DIS process

In the radiative DIS process $-q^2$ is large $(-q^2 \simeq 3.5 GeV^2)$ (off-shell photon) while eighter $-q'^2$,$-q''^2$ is small $(-q'^2 \simeq 0.00015 GeV^2, -q''^2 \simeq 0.3 GeV^2)$ (qusi-real electron). This domain is dominated by the inelastic channel. As $-q^2$ is large, the scattered electron or the $(e - \gamma)$ system a large draction of the produced hadrons is detected. The transverse momentum of the hadronic system is balanced by the transverse momentum of the electron ($e - \gamma$ system). The angular distribution of radiated photons in DIS exhibits two peaks around the direction of the incident and of the scaterred electron corresponding to the regions of small $-q'^2$ and small $-q''^2$. Most of the radiative photons emitted in the direction of the scattered electrons of energy $E'_e \geq 10$ GeV can not be resolved in the H1 detector. However a sizeable fraction of events with radiative photons emitted in the direction of the incoming electrons can be identified in tehe H1 detector. The effective electron beam energy can be determined directly from the measured radiative photon energy E_γ:

$$E_t = E_e - E_\gamma \tag{9}$$

The NC-DIS (including radiative inelastic scattering, also called inelastic Compton scattering) and elastic Compton processes are simulated with the DJANGO [8] and WABGEN [9] generators respectively.

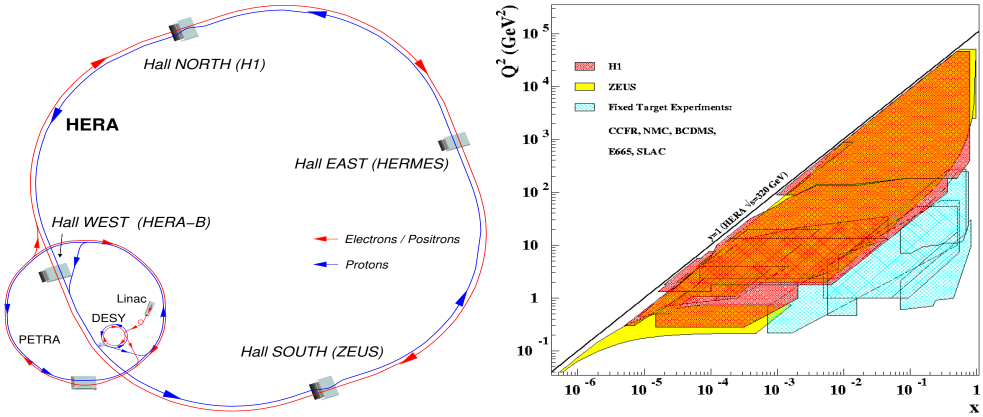

Figure 3: The HERA complex: the scheme including the injectors (left) and the kinematic plane accessible at HERA compared to former fixed target experiments (right).

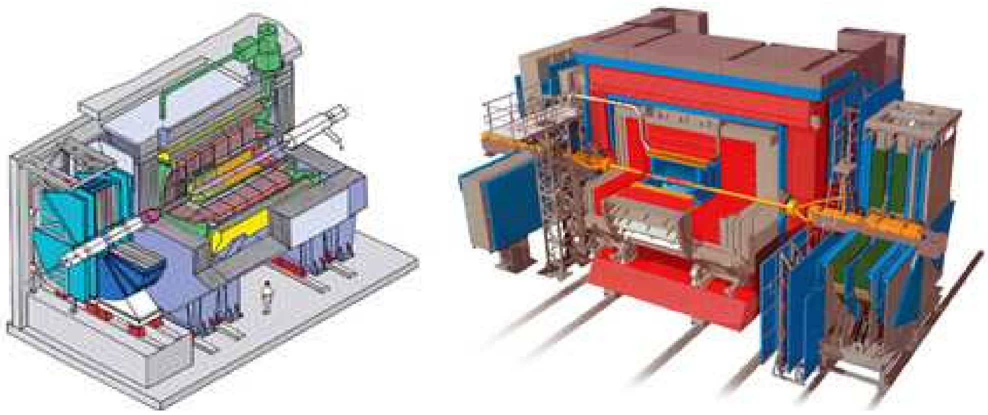

Figure 4: The two collider mode detectors at HERA: H1 (left) and ZEUS (right).

2 The HERA project

2.1 The collider

The idea for a large electron–proton collider to mark a new step in the studies for proton structure was promoted in the seventies [4]. The HERA collider project started in 1985 and produced the first electron–proton collisions in 1992. A scheme of the accelerator complex is shown in figure 3. It is composed of two accelerators designed to store and collide counter rotating electrons (e^-), or positrons (e^+), with an energy of 27.5 GeV and protons with an energy of 920 GeV. The centre–of–mass energy is 320 GeV, equivalent to a hypothetical fixed target experiment with a lepton beam energy of $E \simeq 50$ TeV. The kinematic (x, Q^2) plane accessible at HERA is shown in figure 3 (right) with a Q^2 domain up to about 50000 GeV^2 and x down to 10^{-5}. HERA complements the other high energy colliders Tevatron (Fermilab, Chicago, $p\bar{p}$, $\sqrt{s} = 1960$ GeV)and LEP (CERN, Geneva, e^+e^-, until 2000, $\sqrt{s}$ up to 209 GeV). The next accelerator, the Large Hadron Collider (LHC), will start operations in 2008 and is expected to collide two proton beams at a centre-of-mass energy of 14 TeV.

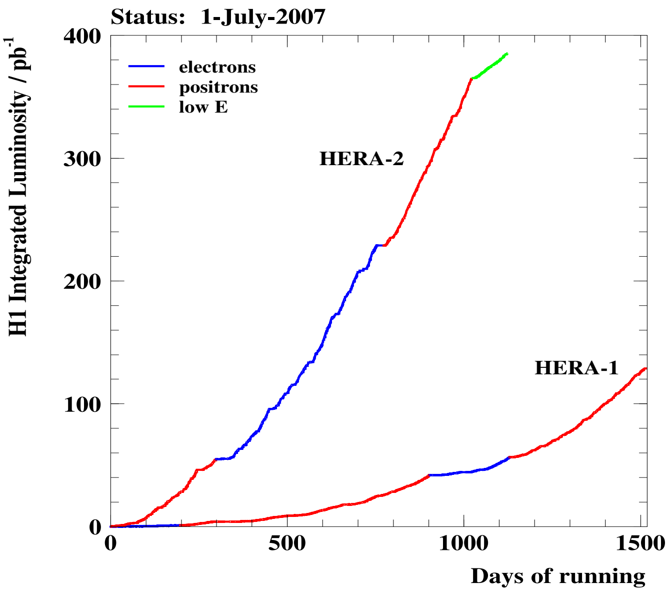

Figure 5: The integrated luminosity as a function of time collected at HERA in electron– and positron–proton collisions.

2.2 The detectors

The HERA ring serves two collider detectors H1 and ZEUS (shown in They are built as hermetic (4π) multi-purpose detectors equipped with inner trackers able to measure charged particle momenta and calorimeters completing the measurement of the energy flow in events from electron–proton collisions. Two further experiments use $e^{\pm}$ or p beams for fixed target studies: HERMES is dedicated to the study of polarised $e^{\pm}p(N)$ collisions and (until 2003) HERA-B was built to study beauty production in hadronic collisions. Since 2003, the $e^{\pm}$ beam is longitudinally polarised with an average polarisation in collision mode of $P_{e^{\pm}} = 30 - 40$ %. HERA collisions will continue until July 2007. An integrated luminosity of 300 pb^{-1} (200 pb^{-1}) is about to be collected in $e^{+}p$ ($e^{-}p$) by each of the two collider mode experiments, H1 and ZEUS. The integrated luminosity as a function of time at HERA is shown in figure 5. A detailed description of the H1 detector can be found in [1]. Only components essential for this analysis are shortly described here[1]. A tracking system of central and forward drift chambers is used to measure the charged particle trajectories and to determine the interaction vertex. Particle transverse momenta are determined from the curvature of the trajectories in a magnetic field of 1.15 Tesla.

Hadronic and electromagnetic final state particles are absorbed in a highly segmented liquid argon calorimeter [2] covering the polar angular range $4° < \theta < 153°$. The calorimeter is 5 to 8 hadronic interaction lengths deep depending on the polar angle of the particle. It includes an electromagnetic section which is 20 to 30 radiation lengths deep. Electromagnetic shower energies are measured with a precision of $\sigma(E)/E = 12\,/\sqrt{E/\mathrm{GeV}} \oplus 1$ and hadronic shower

[1]The origin of the H1 coordinate system is the nominal ep interaction point. The direction of the incoming proton defines the z-axis for the measurement of polar and azimuthal angles as well as for transverse momenta. It also defines the forward region of the detector.

energies with $\sigma(E)/E = 50\sqrt{E/\mathrm{GeV}} \oplus 2$ as measured in test beams [3]. The electromagnetic energy scale is known to the level of 0.7 to 3% depending on the polar angle. The hadronic energy scale is understood at the 2% level.

In the backward region the liquid argon calorimeter is completed by a lead/scintillating-fibre calorimeter [2][6] covering the range $155° < \theta < 178°$, and by electron and photon taggers located downstream of the interaction point in the electron beam direction. The calorimeter is surrounded by a superconducting coil and an iron yoke instrumented with streamer tubes. Leakage of hadronic showers outside the calorimeter is measured from an analogue charge sampling of the streamer tubes (Tail Catcher).

The analysis is restricted to periods where the central drift chambers, the liquid argon calorimeter and the luminosity system are active and fully operational. For the analysed topologies trigger conditions are derived from the liquid argon calorimeter signals. The trigger efficiency is higher than 95% for events with an electron energy above 10 GeV.

3 Event Selection

The present analysis is based on the data recorded by the H1 detector between the years 2003 and 2007. The analysis selects first a NC-DIS event sample, then searches for photons in these events. The photon production is studied in the elestic and inelastic cases. Finally, events with two photons are found and investigated.

3.1 Neutral Current Deep Inelastic Scattering (NC DIS) event selection.

Preselection

Depending on the overal detector performance, background situation, problems with readout and so on, all runs are classified as ”good”, ”medium” or ”poor”. For this analysis only ”good” and ”medium”. Furthermore, for each run it is checked that all important hardware components are fully operational (supplied by high voltage, HV) and included in readout. These components are the LAr calorimeter and LAr trigger, the central drift chambers (CJC1 and CJC2) and the proportional chambers (CIP and COP), the luminosity system, SpaCal and the ToF system. The information about the high voltage (HV) status of each hardware component during data taking was stored inthe database every 10s. A run is rejected is any any of the relevant detectorscomponent was ”off” for a large fraction of tine. For selected runs an event is accepted only if it appears at a time when all HV were ”on”. NC high Q^2 events are triggered essentially by the prominent signature of the scattered electron in the LAr calorimeter. The related subtriggers used for this analysis are s67 and s75 wich are both based on LAr trigger elements asking for minimul energy deposit in the lectromagnetic section of the Lar calorimeter as well as on some timing and veto requirements. Cosmic and halo muon are efficiently rejected using a set of finding algorithms which identify the events on the basis of their topological patterns of long and narrow signatures in combinations of different detector components.

[2]This device was installed in 1995 replacing a lead-scintillator “sandwitch” calorimeter [1].

Topologial criteria for NC-DIS selection

The NC-DIS events are selected by identifying the scattered electron and applying the following criteria:

- electron identified by electron finding and isolating algorithms [11].
- electron transverse momentum $P_T \geq 10$ GeV or $P_T \geq 5GeV$ if the number of electromagnetic particles ≥ 2
- $E - P_z \geq 35$ GeV. For neutral current events where the only non-detected particles are pointing in the proton beam direction, this quantity equals twice the electron beam energy $(E - P_z)_{tot} = 55GeV$.
- central or forward vertex with $|z_{vtx} - < z_{vtx} > | < 35cm$
- exclude electron candidates detected clsoe to z and ϕ cracks:
  $|\phi_e - n * 45°| < 2°, n = 0, 1, ..., 7, 25cm < z_{LAr} < 15cm$
- $y_e < 0.9$ to exclude the photoproduction.

After this criteria 1864232 events are selected in the HERA II data. The kinematics of the selected events is presented in figure 6. Data are compared with Monte Carlo prediction, dominated by the NC-DIS processes simulated using DJANGO program.The ratio of transverse momenta of the hadrons and electrons to the momentum calculated using double angle method[3] show a good calorimeter calilbration (ratio average to one).

[3]Since the NC DIS events are overconstrained (energy and polar angles of the electron and the hadrons yield four measurements, while only two invariants are unknown, say x and Q^2) the "true" transverse momentum of the event can be calculated from the electron and hadrons polar angles - the so-called "double-angle" method. The transverse momentum calculated using this method is independent of the calorimeter energy scale and can be used to calibrated the calorimeter response to electrons and hadrons, as shown in figure 6.

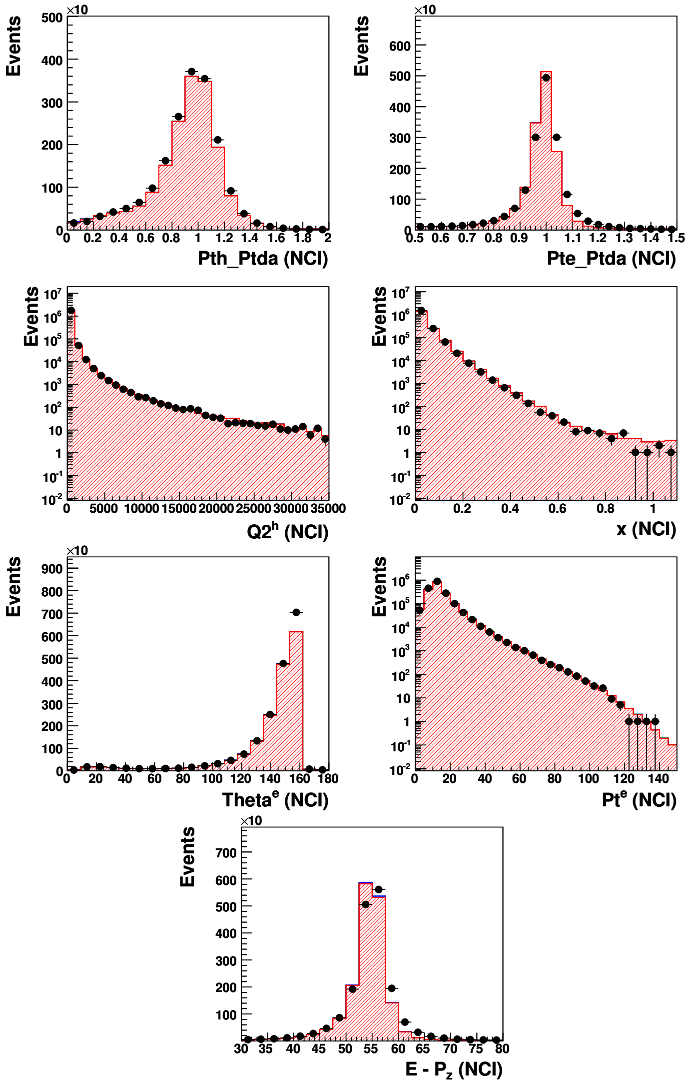

Figure 6: a) Ratio of electron transverse momentum to ”double-angle” transverse momentum, b) Ratio of electron transverse momentum to ”double-angle” transverse momentum, c) Q^2, d) Bjorken scaling variable x, e) Θ distribution of the electron, f) The transverse momentum of the lectron, e) $E - P_z$ for neutral current events

3.2 Multi-photons event selection

A second electromagnetic cluster is searched for in the selected NC-DIS events. The identification starts with the calorimetric based criteria used for electromagnetic particles. Isolation with respect to calorimetric deposits and hadronic jets is then required. Finally, photon candidates matched with signals in the tracking detectors are rejected.

The selection is structured as follows:

A Electromagnetic cluster [4]: - $P_T^{\gamma} > 3GeV$, $5° < \theta^{\gamma} < 150°$

[4] The electromagnetic particles are identified using cluster shape variables and are stored in the class H1PartEm in the H1OO [12] software.

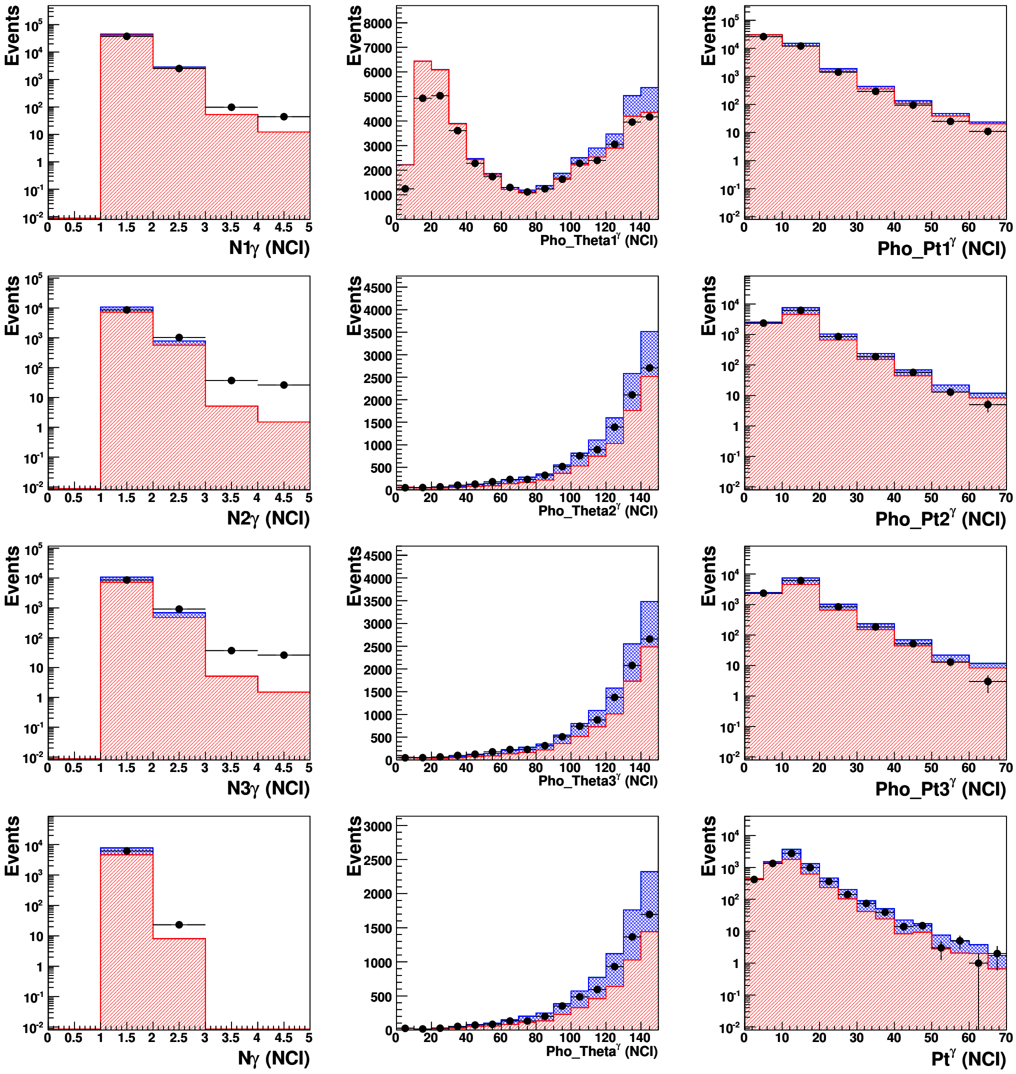

Figure 7: Photon selection steps A, B, C and D (from top to bottom).

- the distance[5] between the photon and the electron $R_{\gamma-e} > 0.5$
- photon candidates detected close to calorimeter cracks are removed.

B Calorimetric isolation:
- the energy detected in the calorimeter in a cone in $\eta - \phi$ of radius 0.5 around the photon candidate should not exceed 2% of the candidate cluster energy.

C Isolation w.r.t. jets:
- the distance between the photon and the closest hadronic jet [6] $R_{\gamma-jet} > 0.5$

D Track veto:
- The track with the smallest distance of closest approach (DCA) to the centre-of-gravity

[5]The distance is calculated in the $\eta - \phi$ plane $R = \sqrt{(\Delta\phi)^2 + (\Delta\eta)^2}$.

[6]Hadronic jets are found using an inclusive k_T algorithm and stored in H1OO software in the calss H1PartKtJet [10].

of the cluster should satisfy $DCA > 24$ cm. Both vertex fitted and non-fitted tracks are considered.
-The distance in $\eta - \phi$ to the closest good quality track should exceed 0.5.

The event yields in data and Monte Carlo is shown in table 1

Photon Selection Steps

Selection	DATA	MC	NC DJANGO	WABGEN
A	39983	48003.1	44269.8	3733.1
B	9701	11508.1	7824.3	3683.7
C	9547	11357.3	7687.9	3669.4
D	6163	7816.9	4634.8	3182.1

Table 1: Event yields at various selection steps (see text).

The distributions of polar angle and transverse momentum and the number of photon candidates are shown in figure 7 for the four selections steps described above. One can observe that without isolationand tracking requirement (step A), an acumulation of photon candidates is observed in the forward direction, corresponding to a fake electromagnetic cluster detected in the hadronic final state of NC-DIS events.

After all cuts, 6163 events NC-DIS are found to have a photon candidate. The prediction of 7816.9 events shows an excess to 20%, not understood at present. The prediction is shared between NC-DIS, mainly modelling the inelastic production (4634.8 events) and WABGEN for the elastic part (3182.1).

The kinematics of the photons are presented in figure 8.

The production of photons takes place via both elastic and inelastic scattering. These event classes can be separated using the hadronic energy measurement in the central detector, measured from particles other than the electron and the photons candidates. The distribution of the hadronic transverse momentum is shown figure 9. It shows a sharp peak close to zero and predicted by the elastic scattering modelled using WABGEN. The prediction exceed the data, therefore one can supose that the global discrepancy is due to a double counting of radiative events between WABGEN and DJANGO, or to an excess of events in which the fake photons contain the full hadronic final state. These questions have not been investigated in depth at present. Events with large hadronic momentum correspond to inelastic scattering and are modelled well by DJANGO. A rough separation of elastic from inelastic events can be performed using a cut $P_T^{had} < 2$ GeV. The distribution of the polar angle of photon candidates for the elastic and inelastic events are also shown in figure 9. Data is well descriebed in shape by the simulation.

3.3 Events with two photons

In figure 7 one can observe that some radiative NC-DIS events contain two (clean) photons. The yield of events at various selection steps is shown in table 2. 23 events present two isolated

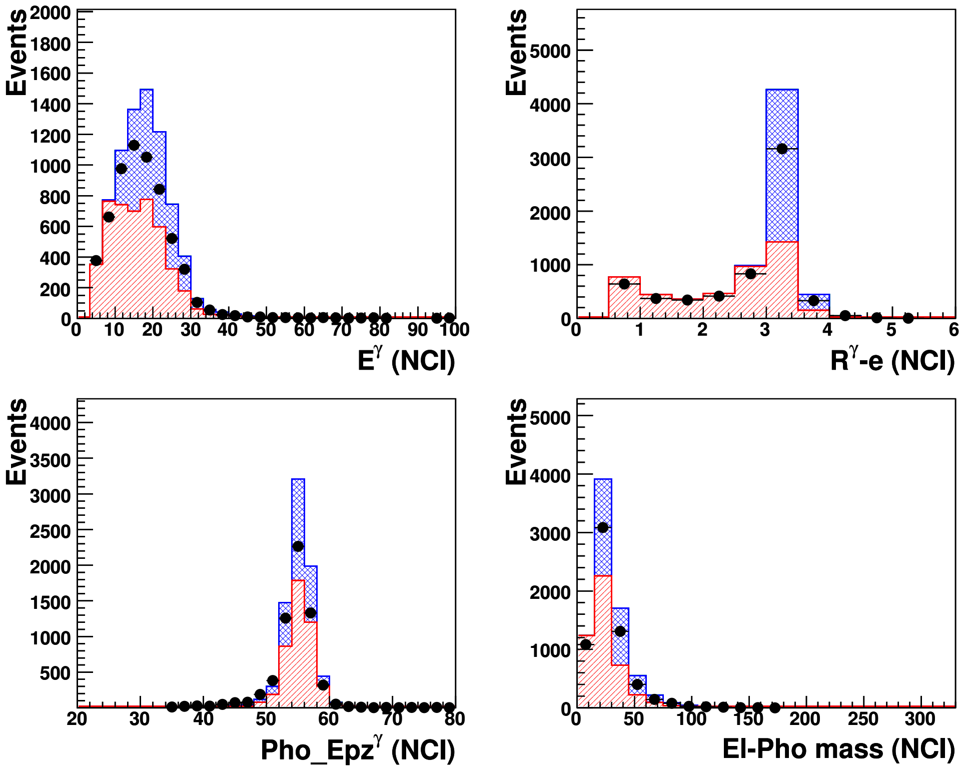

Figure 8: Kinematics of radiative NC-DIS events with a photon detected in the LAr calorimeter: a) The energy distribution of the photons, b) The distance in $\eta - \phi$ plane between the photon and the electron R, c) $E - P_z$ and d) The invariant mass of electron-photon system.

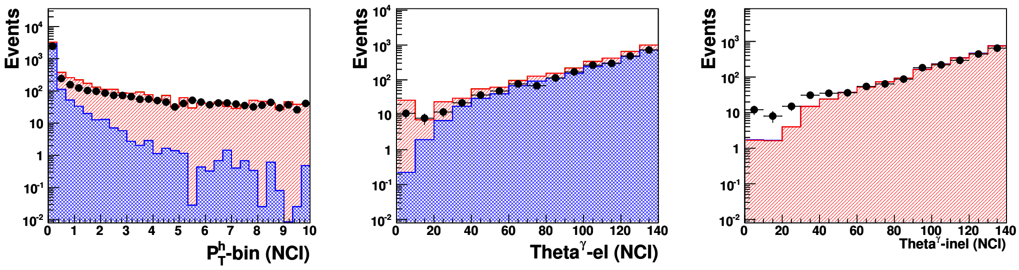

Figure 9: a) The hadronic P_T distribution, b) The polar angle distribution of the elastic Compton process, c) The polar angle distribution of the inelastic Compton process

photons. The events were visually scanned and found compatible with the $e\gamma\gamma$ topology. Their kinematics are listed in the appendix together with the events displays of a few interesting candidates.

The 23 events observed in the data are not properly described by the simulation, with only 8.0 events predicted. This is mainly due to the absence of doubble radiative events in the MC simulation. Nevertheless it would be interesting to know the source of NC-DIS simulation within DJANGO that provide the predicted events. This question has not been further investigated at present.

The kinematic distribution of the two photons are shown in figure 10. Here the photon are

HERA2 Data Multi-photon Analysis

Selection	DATA	MC	NC DJANGO	WABGEN
NC	1864232	1772541.6	1759110.5	13239.7
NC+ γ	6163	7816.9	4634.8	3182.1
NC+ 2γ	23	8.0	8.0	0

Table 2: Yield of events in the selection steps.

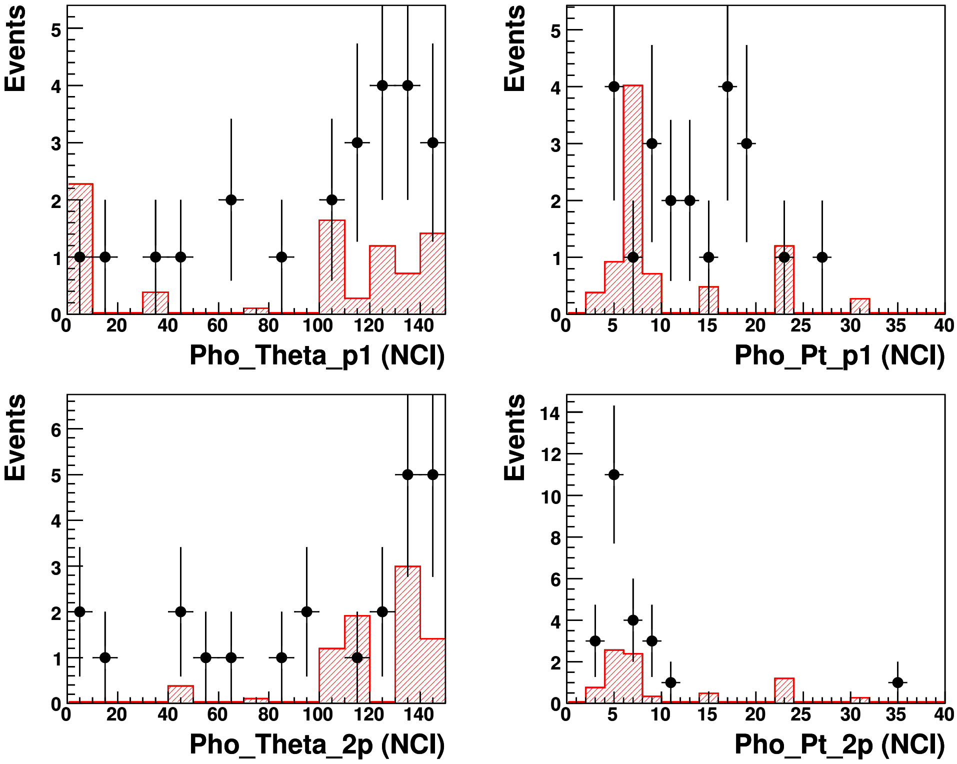

Figure 10: Kinematics distribution of the two photons in $e\gamma\gamma$ events.

ordered in transverse momentum $P_T^{\gamma,1} > P_T^{\gamma,2}$.

In order to study the radiation properties of the bi-radiative events, the distance in $\eta - \phi$ of the photons with respect to the electron and with each other are studied. The distribution of these quantities are shown in figure 11. One can see that when both photons are far away from the electron DJANGO manage some way to describe the shape of data figure 11, a).

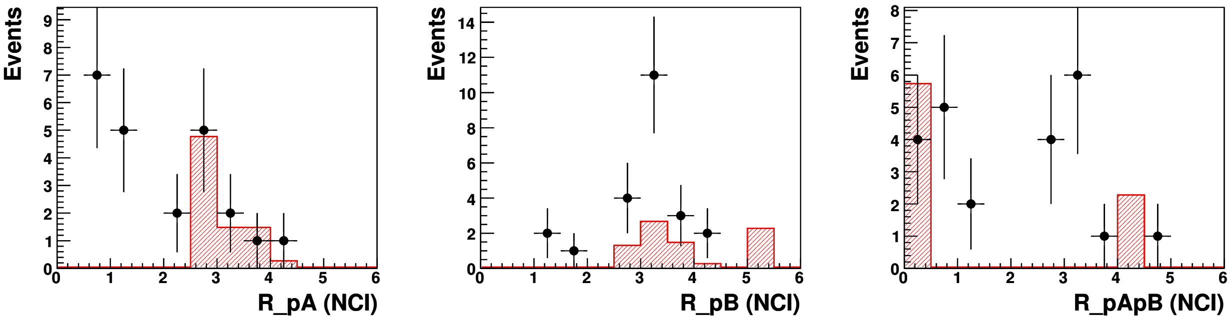

Figure 11: Distances in $\eta - \phi$ between: a) The electron and the closest photon, b) The electron and the farthest photon c) The two photons

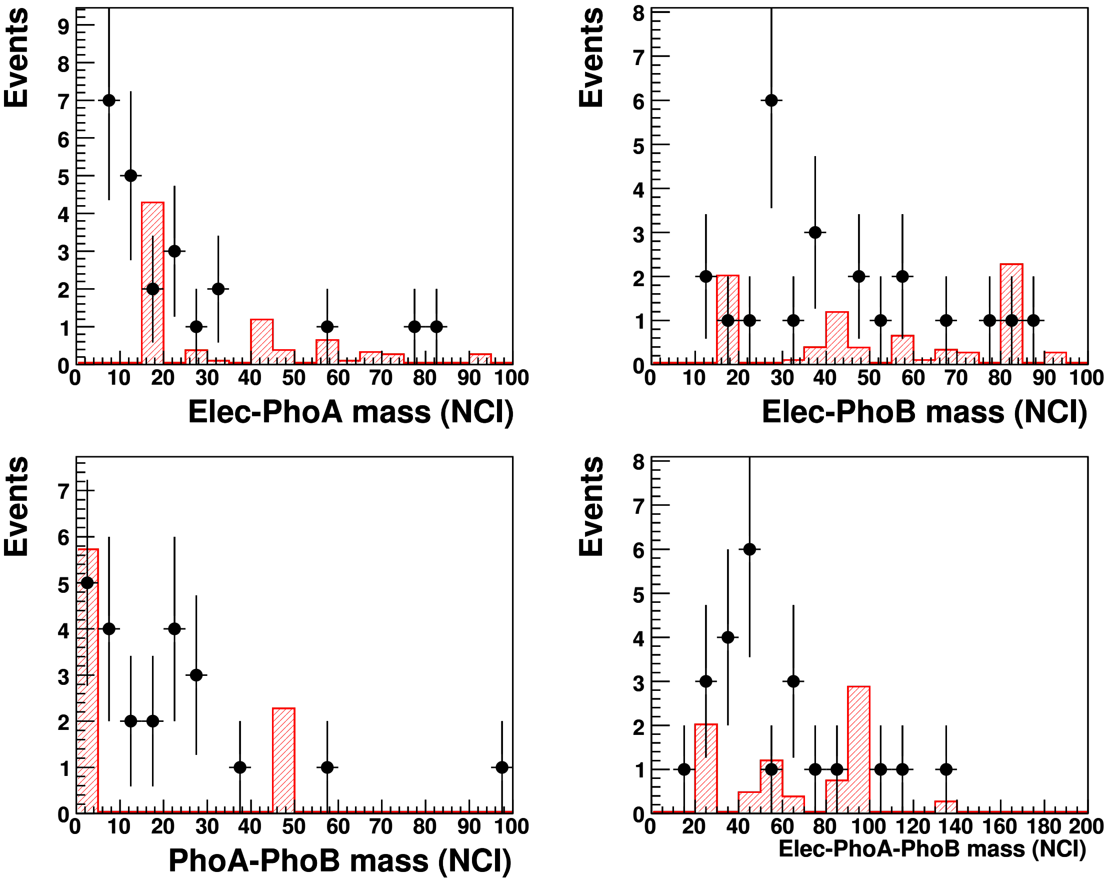

Figure 12: The invariant masses of the: a) Photon closest to electron and electron, b) Photon farthest from electron and electron, c) $\gamma - \gamma$ system, d) $e - \gamma - \gamma$ system

4 Summary and conclusions

Radiative events have been studied using full HERA II data sample collecte by the H1 experiment and corresponding to an integrated luminosity of 350 pb^{-1}. Events with an electron and a photon in the LAr calorimeter have been selected, corresponding to elastic and inelastic Compton scattering.

Events with two photons have been observed with total invariant masses $M_{e\gamma\gamma}$ up to 140 GeV how one can see in figure 12. The rate of such events is not described by the present Monte Carlo generators.

References

[1] H1 Collaboration, I. Abt et al., Nucl. Instr. and Meth. A386 (1997) 310 and 348.

[2] H1 Calorimeter Group, B. Andrieu et al., Nucl. Instr. and Meth. A336 (1993) 460.

[3] H1 Calorimeter Group, B. Andrieu et al., Nucl. Inst. and Meth. A344 (1994) 492; *idem*, Nucl. Instr. and Meth. A350 (1994) 57; *idem*, Nucl. Instr. and Meth. A336 (1993) 499.

[4] A. Febel, H. Gerke, M. Tigner, H. Wiedemann and B. H. Wiik, IEEE Trans. Nucl. Sci. **20** (1973) 782.

[5] C. G. . Callan and D. J. Gross, "High-energy electroproduction and the constitution of the electric Phys. Rev. Lett. **22** (1969) 156.

[6] H1 Spacal Group, R.D. Appuhn et al., Nucl. Instr. and Meth. A386 (1997) 397.

[7] A. Coureau, P. Kessler, Phys. rev. D46, **117**(1992).

[8] DJANGO 2.1; G.A. Schuler and H. Spiesberger, Proceedings of the Workshop Physics at HERA, W. Buchmüller and G. Ingelman (Editors), (October 1991, DESY-Hamburg), vol. 3 p. 1419.

[9] A new Generator for Wide Angle Bremsstrahlung: Ch. Berger and P. Kandel, Proc. of the Monte Carlo Generators for HERA Physics Workshop, DESY-PROC-1999-02, p 596.

[10] S. D. Ellis and D. E. Soper, Phys. Rev. D **48** (1993) 3160 [arXiv:hep-ph/9305266].
C. Adloff *et al.* [H1 Collaboration], Nucl. Phys. B **545** (1999) 3 [arXiv:hep-ex/9901010].

[11] H1 Collaboration, C. Adloff et al., Eur. Phys. J. C5 (1998) 575.

[12] The H1 OO Physics Analysis Project
https://www-h1.desy.de/icas/oop/current/oo.ps.gz

Appendix

HERA2 Data Multi-photon Analysis

Year	0304	05	60	0607
Selection	DATA/MC	DATA/MC	DATA/MC	DATA/MC
NC	265398 / 261649.1	536841 / 524269.4	306185 / 299870.2	755808 / 686753.2
NC+ γ	887 / 1153.7	1844 / 2304.4	981 / 1319.4	2541 / 3039.4
NC+ 2γ	5 / 2.2	10 / 1.7	3 / 0.9	5 / 3.1

Table 3: Evet yield in each data taking period.

Highest invariant mass:

$M_{\gamma-\gamma} = 99.9GeV$

$M_{e-\gamma-\gamma} = 135.1GeV$

Highest Q^2:

Q^2 **= 10444.8**

RUN 381742 Event 69678

Event: E-Pz = 53.76 Ptmiss = 6.53 Q2e = 10444.83 Pth = 0.62

Electron: Pt = 28.65 E = 28.65 Theta = 36.23 Phi = 36.23

Photon: Pt = 69.50 E = 107.38 Theta = 40.33 Phi = -150.19

Photon: Pt = 34.74 E = 34.74 Theta = 56.87 Phi = 56.87

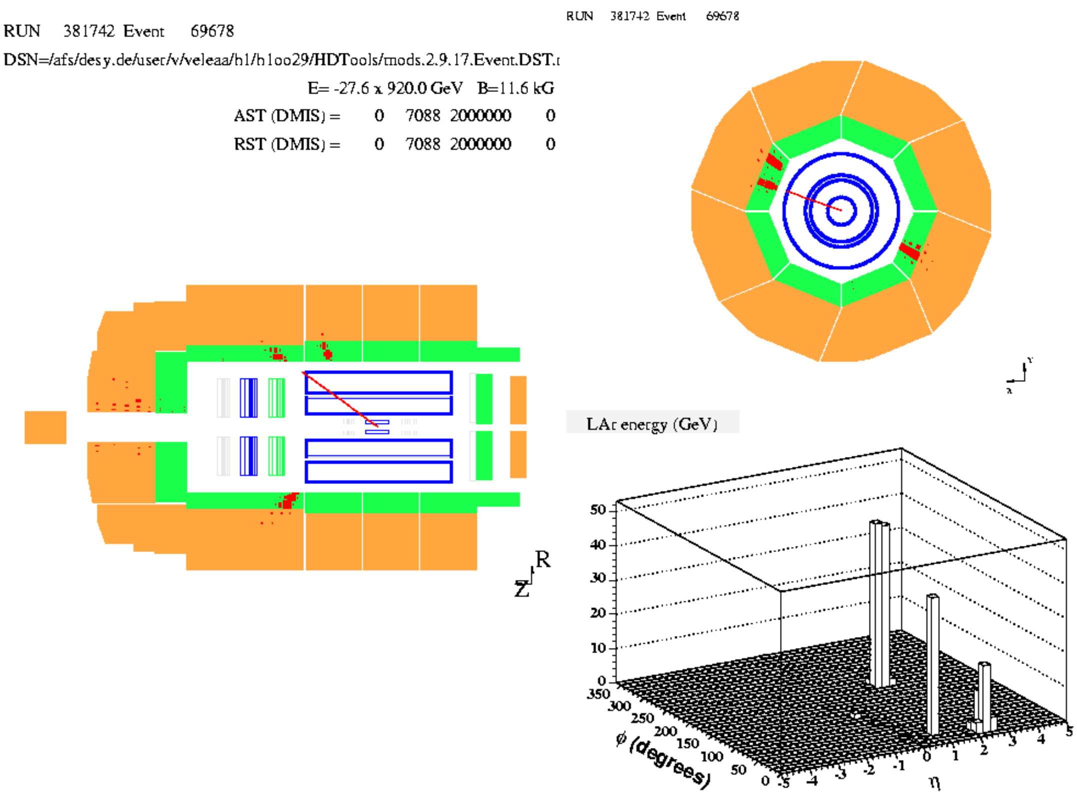

Inelastic event:
Highest P_T^h:
P_T^h **== 28.6 GeV**

RUN 413072 Event 22936

Event: E-Pz = 57.35 Ptmiss = 2.21 Q2e = 2361.57 Pth = 28.61

Electron: Pt = 20.95 E = 26.52 Theta = 52.18 Phi = -66.07

Photon: Pt = 8.99 E = 11.40 Theta = 127.89 Phi = -144.94

Photon: Pt = 6.71 E = 6.78 Theta = 98.26 Phi = -105.23

Jet: Pt = 30.40 Theta = 13.22 Phi = 88.18

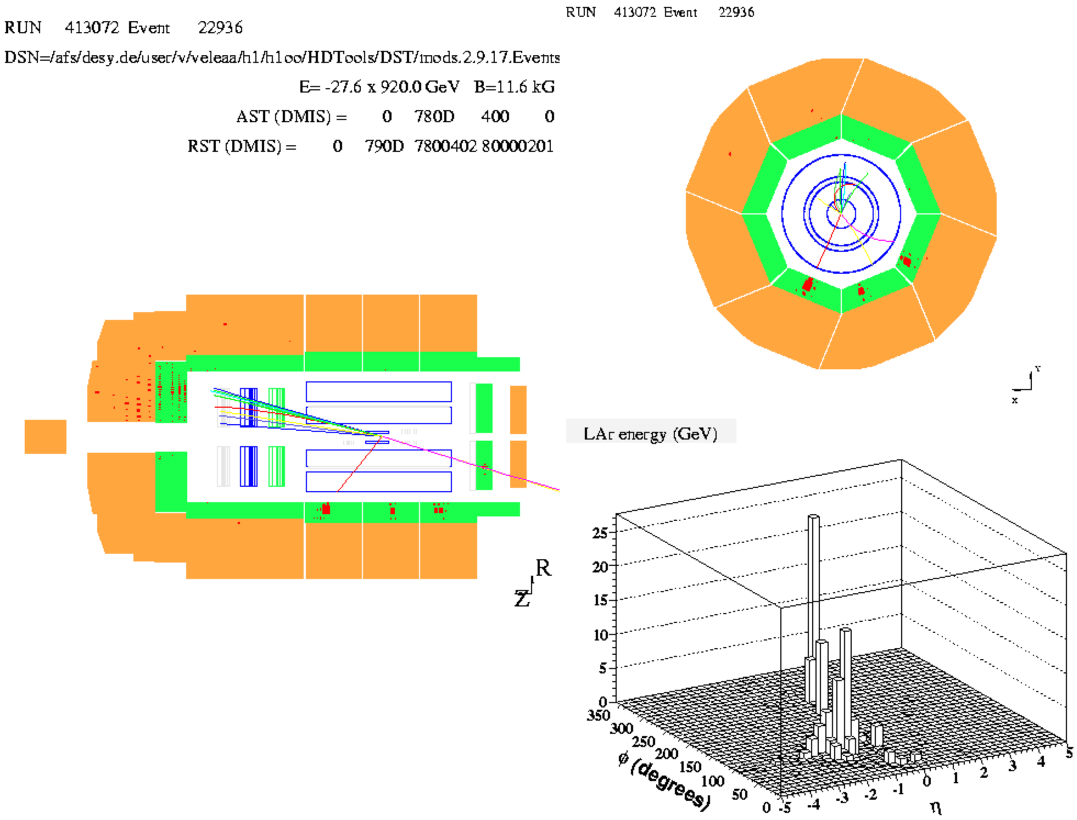

Elastic event:

RUN 424294 Event 82390

Event: E-Pz = 57.35 Ptmiss = 0.27 Q2e = 536.75 Pth = 0.00

Electron: Pt = 15.25 E = 15.70 Theta = 76.27 Phi = -30.46

Photon: Pt = 19.73 E = 24.87 Theta = 127.52 Phi = 160.24

Photon: Pt = 5.63 E = 5.64 Theta = 86.90 Phi = 13.62

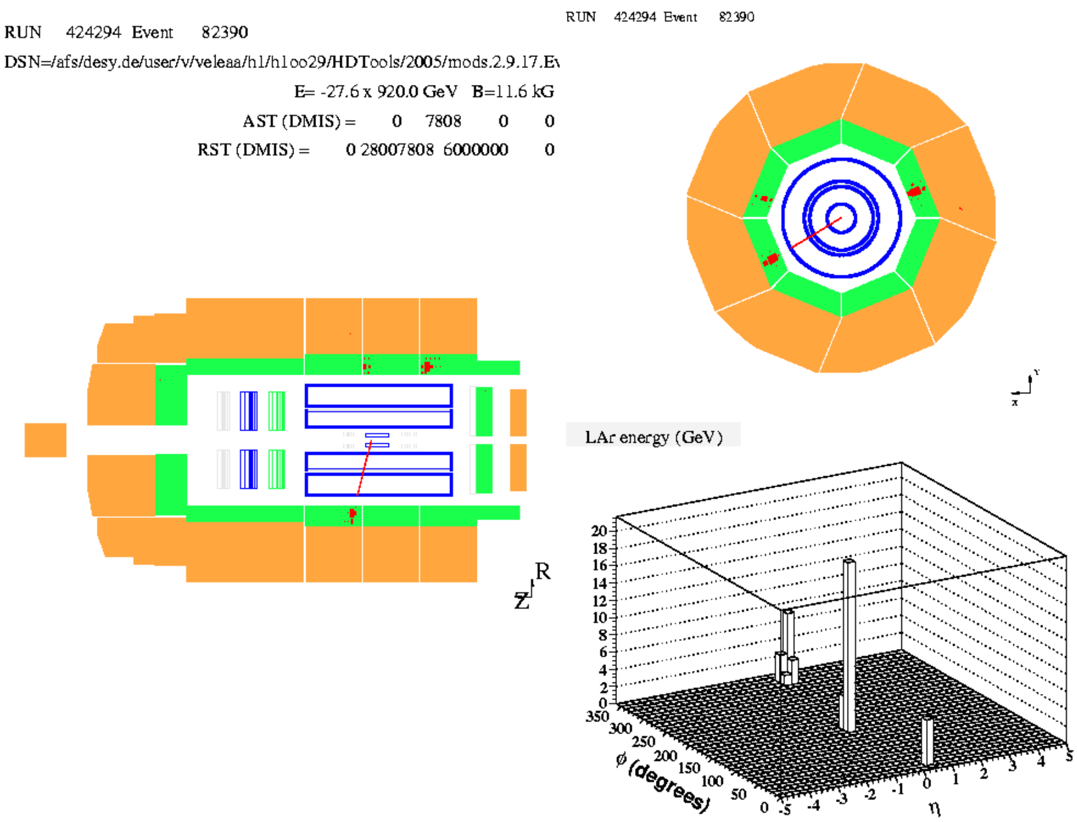

HERA2 Data — Multi-photon Events

RUN/EVENT	e P_t/Θ/Φ	γ_1, γ_2 P_t/Θ/Φ	P_t^{had}/$E-P_z$/P_t^{miss}	$M_{e-\gamma_1}$/$M_{e-\gamma_2}$ $M_{\gamma_1-\gamma_2}$/$M_{e-\gamma_1-\gamma_2}$
369273 30983	13.3/103.4/-20.5	10.0/149.8/128.0 7.6/46.2/-157.7	0.0/57.1/0.9	22.0/25.5 24.9/41.8
375379 131960	19.6/19.6/-37.2	11.6/113.9/113.9 4.6/120.0/-9.0	28.9/49.4/2.0	6.5/18.0 24.9/19.9
381243 49833	27.6/25.6/-17.8	27.6/25.6/-17.8 4.8/118.3/149.9	16.5/54.2/0.7	83.4/83.4 0.0/118.0
381742 69678	28.6/25.6/19.1	69.5/40.3/-150.1 34.7/56.8/36.3	0.6/53.7/6.5	18.6/89.0 99.9/135.1
381843 105097	10.5/85.1/-25.8	16.5/132.8/143.9 4.9/120.2/-65.7	1.95 /56.2/1.95	6.8/28.8 17.7/34.5
413072 22936	20.9/52.1/-66.0	8.9/127.8/127.8 6.7/98.2/-105.2	28.6/57.3/2.2	13.0/27.1 6.7/30.9
418620 142260	15.0/56.8/112.4	12.7/114.2/-85.2 11.2/133.3/126.2	13.1/55.3/2.1	20.6/31.1 23.2/44.0
421037 148018	15.5/123.6/-20.2	19.5/65.8/153.7 4.3/141.1/-47.4	0.0/54.0/0.1	5.3/39.9 24.1/47.0
424294 82390	15.5/123.6/-20.2	15.2/76.2/-30.4 19.7/127.5/160.2	0.0/57.3/0.2	7.1/38.1 21.5/44.4
428817 6093	20.6/91.0/-53.8	26.5/39.9/124.4 4.3/149.1/-51.4	0.0/46.4/1.8	12.9/53.1 37.6/66.4
429613 42017	11.9/106.6/-154.4	9.7/137.3/42.1 3.4/144.6/-12.2	0.0/51.9/0.6	13.4/22.5 5.4/26.8
406087 76728	14.6/48.5/-162.6	14.7/135.9/55.5 3.5/147.6/-115.3	3.6/55.7/4.9	18.2/39.3 14.5/45.7
435736 138798	12.5/18.1/-113.0	16.3/146.8/73.9 3.6/7.2/-81.1	0.0/57.0/0.5	7.4/68.1 56.6/88.8
436879 131140	11.4/36.4/21.1	16.2/143.0/-170.9 5.0/47.9/-22.0	0.0/54.5/0.8	6.0/45.5 26.5/53.0
4088519 137552	12.7/49.8/-175.6	12.5/129.9/-54.3 9.2/133.7/-19.8	8.8/54.9/5.8	16.6/29.0 6.4/42.5
450762 31825	21.9/37.6/72.6	19.8/123.1/-125.3 7.8/95.0/-47.6	0.0/52.7/1.1	27.8/56.4 16.7/65.1
456060 39126	10.5/21.7/-86.2	23.1/109.1/-86.2 8.7/134.8/-119.2	0.0/55.6/5.4	31.2/47.4 28.7/63.6
466954 24009	15.9/16.9/75.2	5.9/13.3/-21.3 17.1/140.6/-127.7	1.2/78.5/1.9	75.1/75.1 0.0/106.3
477217 14241	16.2/36.8/-171.9	4.3/6.3/-103.7 19.2/138.8/18.9	0.0/56.9/1.1	56.2/56.2 0.0/79.4
481397 55850	12.3/150.1/-73.2	6.3/63.5/111.2 5.7/68.6/94.8	0.4/54.8/1.2	23.7/25.7 1.8/35.0
488387 158717	10.7/71.2/-111.3	9.2/107.1/-55.8 8.6/136.0/-132.4	22.9/52.6/1.5	11.2/13.0 12.1/21.1
488455 321898	10.4/112.7/39.1	17.4/89.0/-139.0 7.0/145.2/31.0	0.0/55.4/1.5	6.7/27.5 25.9/38.4
494988 67344	10.4/142.6/36.0	5.3/130.2/-112.9 4.9/133.2/-155.1	0.3/53.9/1.2	14.3/14.4 3.6/20.6

Table 4: Event kinematics.